Applied Catalysis B: Environmental 142–143 (2013) 354–361

Contents lists available at SciVerse ScienceDirect

Applied Catalysis B: Environmental

journal homepage: www.elsevier.com/locate/apcatb

Catalytic reduction of nitrate in water over Pd–Cu/TiO_2 catalyst: Effect of the strong metal-support interaction (SMSI) on the catalytic activity

Min-Sung Kim[a], Sang-Ho Chung[a], Chun-Jae Yoo[a], Myung Suk Lee[a], Il-Hyoung Cho[c], Dae-Won Lee[a,*], Kwan-Young Lee[a,b,**]

[a] Department of Chemical and Biological Engineering, Korea University, 5-1, Anam-dong, Seongbuk-Gu, Seoul 136-713, Republic of Korea
[b] Green School, Korea University, 1-5, Anam-dong, Seongbuk-Gu, Seoul 136-713, Republic of Korea
[c] Department of Environmental and Energy Systems Engineering, Kyonggi University, Gyeonggi-Do, Republic of Korea

ARTICLE INFO

Article history:
Received 25 February 2013
Received in revised form 26 April 2013
Accepted 16 May 2013
Available online 25 May 2013

Keywords:
Nitrate reduction
SMSI
Pd–Cu/TiO_2
H_2-TPR
XPS

ABSTRACT

In this study, we prepared TiO_2-supported Pd–Cu catalysts of different anatase/rutile phase compositions, which were used in a nitrate reduction in water. It was shown that the catalysts containing a greater anatase phase composition had higher catalytic performance. Through characterization studies using H_2-temperature programmed reduction (H_2-TPR) and X-ray photoelectron spectroscopy (XPS), the observed trend of the catalytic activity was correlated to the degree of the strong metal-support interaction (SMSI) over the catalysts. The SMSI occurred through pre-treatment of the catalysts by H_2 reduction (at 200 °C), which resulted in increased partially reduced TiO_{2-x} and electron-rich active metal (Pd and Cu) states at the catalyst of higher composition of anatase phase. The relationships between the changes in the properties and activities of the catalysts as a result of the anatase phase composition are discussed.

1. Introduction

In water, nitrate (NO_3^-) is considered a potentially hazardous material that is emitted from various sources including: natural circulation of nitrogen, waste materials in industries, row crop agriculture and irrigated agriculture [1,2]. Nitrate converted to nitrite by microbes can lead to harmful effects on the human body, such as liver damage, cancers and blue baby syndrome [3,4]. To diminish the health risk, the allowable level of nitrate in drinking water is fixed at 10, 25 and 50 ppm by the United States Environmental Protection Agency, the World Health Organization and the European Community, respectively [5]. With constantly increasing concerns for the stringent regulation of nitrate, nitrate removal technologies are a constant need in populated regions. The available methods for nitrate removal include physicochemical treatments such as reverse osmosis, electrodialysis and ion exchange [6,7], but none of these methods are a universal and definite solution because the treated samples need further to address the brine produced in these methods [8,9]. Biological methods have also been applied for nitrate removal [6,7,10], but they have their own limitations including bacterial contamination and the presence of remaining organic compounds in the treated water [11]. To improve above the available methods, a catalytic reduction method was suggested by Vorlop and Tacke [12], which is an efficient and economical method that enables high nitrate conversion under relatively mild conditions [13]. The catalytic reduction of nitrate can occur as follows [14]:

$$NO_3^- + H_2 \rightarrow NO_2^- + H_2O$$

$$2NO_2^- + 3H_2 \rightarrow N_2 + 2H_2O + 2OH^-$$

$$NO_2^- + 3H_2 \rightarrow NH_4^+ + 2OH^-$$

Nitrate is reduced to both nitrogen and ammonium ion via nitrite. Of course, nitrogen is the desired product in the method.

As has been reported in numerous studies, the catalytic activity of palladium or platinum loaded catalysts in nitrate reduction significantly enhanced by promoter like copper [15–18]. Among them, Pd–Cu pair catalysts showed the higher activity for nitrate conversion and for N_2 selectivity than Pt–Cu pair [19–23]. Meanwhile, many authors aimed to search for the suitable support materials to promote the catalytic performance of Pd–Cu such as activated-carbon [24,25], fibrous carbon [26], polymer resin [27], Al_2O_3 [28], combinated MeO_x–Al_2O_3 [29] and TiO_2 [30]. Recently,

* Corresponding author. Tel.: +82 2 3290 3727; fax: +82 2 926 6102.
** Corresponding author at: Department of Chemical and Biological Engineering, Korea University, 5-1, Anam-dong, Seongbuk-Gu, Seoul 136-713, Republic of Korea. Tel.: +82 2 3290 3299; fax: +82 2 926 6102.
E-mail addresses: stayheavy@korea.ac.kr (D.-W. Lee), kylee@korea.ac.kr (K.-Y. Lee).

0926-3373/$ – see front matter © 2013 Elsevier B.V. All rights reserved.
http://dx.doi.org/10.1016/j.apcatb.2013.05.033

Table 1
Chemical composition and BET properties of Pd–Cu/TiO_2 catalysts.

Abbreviation	Catalyst	Pd [Cu] content[a] (wt.%)	Surface area[b] (m^2/g)	Pore volume[b] (cm^3/g)
PCT500	Pd–Cu/TiO_2 (500 °C)	2.6 [1.0]	12.3	0.030
PCT920	Pd–Cu/TiO_2 (920 °C)	2.5 [0.9]	8.7	0.016
PCT1020	Pd–Cu/TiO_2 (1020 °C)	2.5 [0.9]	3.4	0.003

[a] Determined by ICP-AES.
[b] Estimated by BET.

the main focus for the effective TiO_2-supported catalysts has been on optimizing the properties of metal species (e.g., improving the Pd–Cu contact) through applying the modified or different methods in preparing the catalysts (e.g., liquid-phase chemical reduction, photo-deposition) [30–32]. However, there are few studies investigating about the influence of metal-support interaction on the activity of Pd–Cu/TiO_2 catalyst for nitrate reduction. Thus, it is necessary to figure out the dependence of the active metal (Pd–Cu) properties on the crystalline phase of the support material (TiO_2).

Generally, TiO_2 exhibits SMSI (strong metal-support interaction) with Group VIII metals [33]. It is well known that SMSI can occur when the catalyst is reduced by hydrogen [34,35]. H_2 reduction over TiO_2-supported catalysts generates oxygen vacancies in the form of coordinatively unsaturated cations in the vicinity of active metals, which leads to changes in the catalytic activity and stability [36–41]. These phenomena were largely dependent on the TiO_2 phase: Li et al. noted that the treatment of the Pd/TiO_2-anatase phase by H_2 reduction at low temperature (200 °C) led to higher reactivity in hydrogenation of alkadienes than that of the Pd/TiO_2-rutile phase because SMSI was observed only in the anatase phase-supported catalyst [42]. On the other hand, the SMSI between Ni and the rutile phase over Ni/TiO_2 catalysts was the main reason for the enhanced activity of the catalysts in acetophenone hydrogenation [43].

Our objective in this study is to investigate the influence of SMSI on catalytic nitrate reduction over Pd–Cu/TiO_2 catalysts. The catalysts were prepared by the deposition-precipitation method in which palladium and copper are simultaneously incorporated onto TiO_2. We tested anatase, rutile and mixture of both phases as the TiO_2 supported for Pd–Cu. We concentrated on the characterization of the prepared catalysts using X-ray diffraction (XRD), H_2-temperature programmed reduction (H_2-TPR) and X-ray photoelectron spectroscopy (XPS), and tried to relate the results to the catalytic activity.

2. Experimental

2.1. Preparation of catalysts

Different anatase/rutile phase compositions of TiO_2 supports were prepared through the calcination of pure anatase TiO_2 (Aldrich, 99.8%) at 500, 920 and 1020 °C for 4 h in air [44]. Each support was designated as T500, T920 and T1020. The TiO_2-supported Pd–Cu catalysts were synthesized by a deposition-precipitation method [45,46]. In this method, 10 g of the TiO_2 supports was suspended in 300 ml of 0.01 M of HCl aqueous solution. Then, palladium chloride ($PdCl_2$, Aldrich, 99.5%) and copper chloride ($CuCl_2$, Aldrich, 97%) were added. In all of the catalyst preparations, the Pd and Cu loadings were fixed at 2.5 and 1 wt.%, respectively. The compositions of Pd and Cu were determined by preliminary reaction tests (under a pure hydrogen flow) that were carried out with varying the contents of Cu in 2.5 wt.% Pd–Cu/TiO_2(500) catalysts. In this test, the catalyst of 2.5 wt.% Pd–1 wt.% Cu showed the highest N_2 selectivity among the tested catalysts (data not shown). The pH of the precursor solution was adjusted to 10 using an aqueous solution of Na_2CO_3 (1 M), and the solution was vigorously stirred at 70 °C for 21 h. Afterwards, the resulting solution was filtered and washed with deionized water until no chlorides were detected by an addition of a silver nitrate solution. After drying at 100 °C for 24 h, the catalysts were calcined in air at 300 °C for 6 h. Before the reaction tests, all of the catalysts were reduced in H_2/N_2 (10 vol.%) at 200 °C for 2 h. The abbreviations, BET properties and chemical compositions (estimated by ICP-AES) of the catalysts are listed in Table 1.

2.2. Characterization of catalysts

The surface area and pore volume of the catalysts were analyzed by the N_2 adsorption-desorption method on a BET instrument (Micrometrics, ASAP 2010). Before the measurements were taken at 77 K, catalysts were degassed at 573 K and 4 mmHg.

The contents of Pd and Cu in the Pd–Cu/TiO_2 catalysts were determined by inductively coupled plasma atomic emission spectroscopy (ICP-AES, Poly Scna 61 E, ELTRA ONH 2000).

X-ray diffraction (XRD) patterns were taken on an X-ray powder diffractometer (Rigaku DMAX-2500) using Cu Kα (λ = 1.5406 Å) irradiation. The data were collected in the 2θ range of 20 to 85° at a scanning rate of 1°/min.

H_2-temperature programmed reduction (TPR) analysis was performed on a BELCAT-M-77 instrument (BEL Japan Inc.). The catalyst was enclosed in a quartz tube and purged at 200 °C for 30 min in flowing He (30 ml/min) and then cooled down to 25 °C. The TPR data were collected with increasing the temperature from 25 °C to 750 °C (heating rate: 10 °C/min) in a flow of 5% H_2/N_2 (50 ml/min).

X-ray photoelectron spectroscopy (XPS) experiments were performed on a PHI 5000 VersaProbe with an Al Kα X-ray source (1486.6 eV), and all of the binding energies were calibrated with the reference of C1s binding energy at 284.6 eV. The core electrons of Ti 2p, Pd 3d and Cu 2p were detected.

2.3. Activity test

The catalytic activities were measured on a semi-batch reactor where Pd–Cu/TiO_2 catalysts were suspended in nitrate-dissolved water. The experiments were performed with stirring the reactor (700 rpm) at 25 °C and atmospheric pressure. Hydrogen was used as reducing agent and fed to the reactor continuously (90 ml/min). The catalyst (0.15 g) was added into 295 ml of deionized water and purged with N_2 and H_2. Then, 5 ml of solution containing 2 mM nitrate reactant was fed into the reactor. In some cases, CO_2 gas was used as a pH buffer to acquire higher N_2 selectivity.

During the reaction test, the samples (1 ml, each) were collected to estimate the concentrations of nitrate, nitrite and ammonium ions. The nitrate and nitrite ions were quantified using an HPLC (Young-Lin) with a UV detector at a wavelength of 210 nm and a Zorbax Eclipse C18 column under isocratic conditions. Octylammonium orthophosphate (0.01 M) and pure methanol were used as the mobile phase. The ammonium ions were quantified using an IC (Dionex, TCD detector) equipped with an IonPac CS12A column. The mobile phase was 20 mM of methanesulfonic acid.

Table 2
Anatase phase composition of Pd–Cu/TiO_2 catalysts.

Material		PCT500	PCT920	PCT1020
Weight fraction of anatase (%)	Calcined	98	75	1
	Reduced	98	75	1

Nitrate (NO_3^-) conversion was calculated based on Eq. (1).

$$\text{Nitrate Conversion, } X(NO_3^-)(\%) = \frac{C(NO_{3,t=0}^-) - C(NO_3^-)}{C(NO_{3,t=0}^-)} \times 100 \quad (1)$$

The selectivities of nitrite (NO_2^-), ammonium (NH_4^+) and nitrogen (N_2) were calculated using equations (2), (3) and (4).

$$\text{Nitrite Selectivity, } S(NO_2^-)(\%) = \frac{C(NO_2^-)}{C(NO_{3,t=0}^-) - C(NO_3^-)} \times 100 \quad (2)$$

$$\text{Ammonium Selectivity, } S(NH_4^+)(\%) = \frac{C(NH_4^+)}{C(NO_{3,t=0}^-) - C(NO_3^-)} \times 100 \quad (3)$$

$$\text{Nitrogen Selectivity, } S(N_2)(\%) = 100 - S(NO_2^-) - S(NH_4^+) \quad (4)$$

In these equations, $C(NO_{3,t=0}^-)$ is the initial concentration of nitrate, and $C(NO_3^-)$, $C(NO_2^-)$ and $C(NH_4^+)$ are the concentrations of the corresponding components in the collected sample. $S(N_2)$ is obtained for the nitrogen-balance equation between the reactants and the products.

3. Results and discussion

3.1. BET, ICP-AES and XRD analysis

The BET surface area and pore volume of the Pd–Cu/TiO_2 (PCT) catalysts are shown in Table 1. The BET surface areas of PCT500, PCT920 and PCT1020 were 12.3, 8.7 and 3.4 m^2/g, respectively, and were found to decrease as the calcination temperature of the TiO_2 support increased. The pore volume also displayed a similar tendency depending on the catalysts. The amount of Pd and Cu was measured using ICP-AES. All of the catalysts showed similar values (~2.5 and ~1.0 wt.%) in Pd and Cu content.

Fig. 1(b) presents the XRD profiles of calcined PCT catalysts. The XRD patterns exhibited the typical lines of the anatase (2θ = 25, 37, 48, 53, 55, 62, 71°) or rutile phase (2θ = 27, 36, 39, 41, 44, 54, 56, 64, 68°), indicating that the TiO_2 support retained its initial structure even after Pd and Cu were loaded. The anatase phase composition was calculated by using Eq. (5).

$$X_A(\%) = \left[1 + 1.26\left(\frac{I_R}{I_A}\right)\right]^{-1} \times 100 \quad (5)$$

I_R means the intensity of the strongest diffraction peak (1 1 0) of the rutile phase. I_A indicates the intensity of the strongest diffraction peak (1 0 1) of the anatase phase. As the calcination temperature of the TiO_2 supports increased, the pure anatase phase was transformed into the rutile phase (Table 2). The Cu oxide-related phases were not observed in the XRD profiles, whereas a very broad diffraction peak of the Pd oxide phase (PdO [1 0 1]; 2θ = 34.4°) was observed in the magnified XRD patterns (Fig. 1(b)).

The reduced PCT catalysts had the anatase fractions of the TiO_2 supports almost identical to the pre-reduced catalysts (Fig. 2), which might be caused by the low reduction temperature (200 °C; The bulk reduction of TiO_2 is known to occur above 400 °C). Similarly, there was no metallic Cu or Cu oxide phases observed on the XRD results (Fig. 2(a)). The absence of Cu-related phases is considered to be due to the low Cu-loading amount (1 wt.%), which was

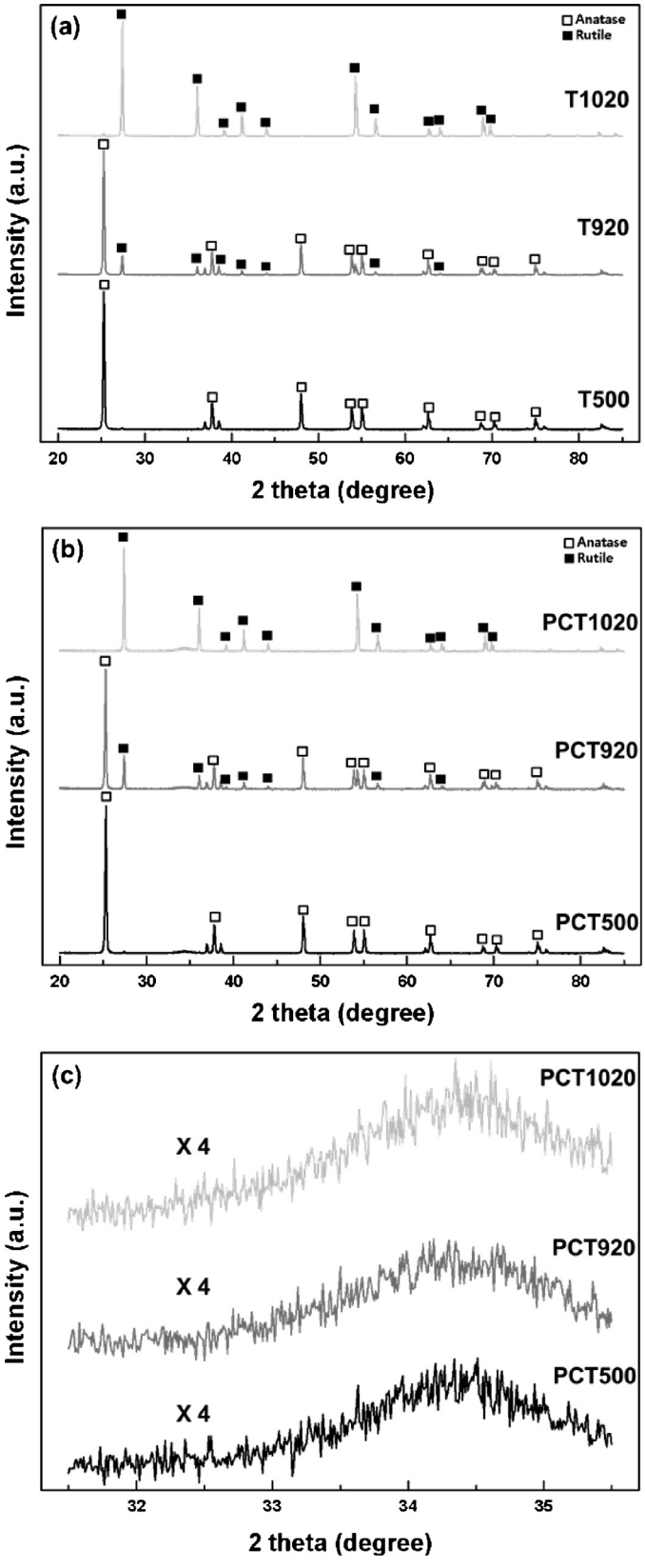

Fig. 1. (a) XRD patterns of the calcined TiO_2 supports; (b) XRD patterns; (c) magnified XRD patters (2θ: 31.5–35.5°) of the calcined Pd–Cu/TiO_2 catalysts.

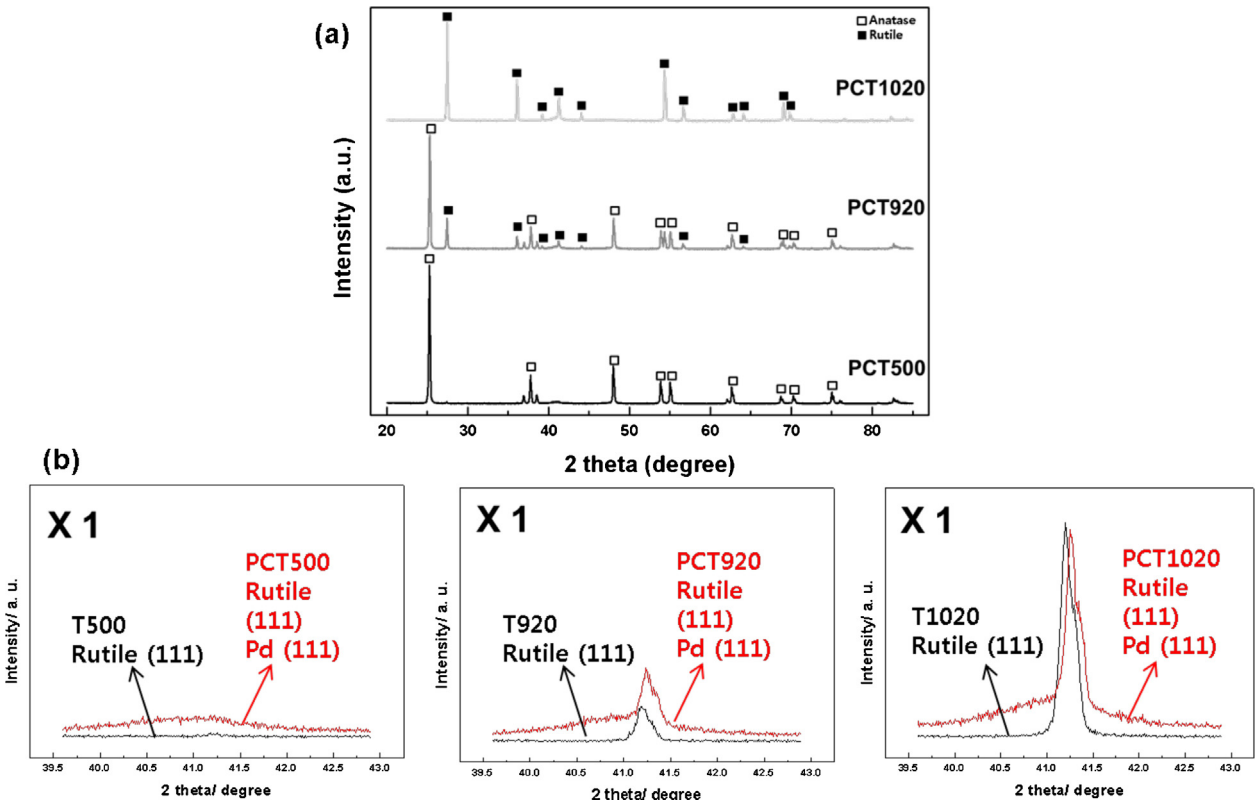

Fig. 2. (a) XRD patterns; (b) magnified XRD patters (2θ: 39.7–42.8°) of the reduced Pd–Cu/TiO_2 catalysts.

below the XRD detection limit. Fig. 2(b) displays the magnified XRD profiles of the TiO_2 supports and PCT catalysts at approximately 41°. In the cases of the PCT catalysts, the intensities of the peaks around 40–42° were higher than those of the bare TiO_2 supports, which suggested that the metallic Pd peaks partially overlapped with the peaks of the rutile phase. Although the growth of Pd metallic phase was observed, the metallic Pd phase could not be precisely discerned due to the broad shape of the peak. The results presented above indicated that the differences in the chemical or crystallographic states of Pd and Cu among the PCT catalysts could not be distinguished using XRD measurements.

3.2. H_2-TPR analysis

Fig. 3(a) represents the TPR profiles of the PCT catalysts. Each PCT500, PCT920 and PCT1020 catalyst showed a peak centered at 109.1, 104.2 and 95.6 °C, respectively. In the cases of PCT500 and PCT920, the negative peak caused by the decomposition of Pd hydride was observed [47,48], whereas a typical (positive) reduction peak of Pd oxide only appeared in the PCT1020 sample. The Pd-hydride reduction peak was shift to a higher temperature with the catalyst including more anatase phase, which could be attributed to the stronger interaction between the metal and support [49]. The different degree of the metal-support interaction over the PCT catalysts was also observed by the TiO_2 reduction pattern above 400 °C (Fig. 3(b)). It is well known that spillover of dissociatively chemisorbed hydrogen on a noble metal promotes the reduction of TiO_2 [31]. This behavior was clearly shown in Fig. 3(b); the order of the amount of hydrogen consumption for TiO_2 reduction was as follows: PCT500 > PCT920 > PCT1020. Furthermore, at PCT500, the maximum TiO_2 reduction peak was found at the lowest temperature (552 °C), which demonstrated that the active metal Pd promotes TiO_2 reduction more vigorously in PCT500 than in the other PCT catalysts. It is expected that the surface of Pd particle was decorated by TiO_2 overlayer during the TPR run as a result of SMSI in PCT500 [48], which would increase the contact between Pd and TiO_2 and then lead to the enhancement of TiO_2 reduction rate. It indirectly supported the previous conclusion that the metal–support interaction is the strongest in PCT500 among the catalysts. On the other hand, it was difficult to recognize the effect of the SMSI on the Cu species because the reduction peak of Cu oxide was not observed in the TPR data.

3.3. XPS analysis

To investigate the surface state of the reduced PCT catalysts, an XPS study was carried out. Fig. 4(a) shows the Ti 2p XPS spectra of PCT catalysts, indicating the different valence states of Ti with anatase composition. For Ti^{4+} (in TiO_2) and Ti^{3+} (in Ti_2O_3), the Ti $2p_{3/2}$ binding energies were 458.6 and 457.8 eV, respectively. In the cases of the PCT500 and PCT920, the Ti $2p_{3/2}$ spectrum could be deconvoluted into two peaks of Ti^{4+} and Ti^{3+}. One peak placed at a lower binding energy could be assigned to Ti^{3+}. The lower binding energy peak of PCT500 (458.1 eV) was closer to the state of Ti^{3+} than that of PCT 920 (458.3 eV). On the other hand, PCT1020 exhibited only one peak at 458.8 eV (Ti^{4+}). Li et al. discovered that the reduction with H_2 at 200 °C resulted in an SMSI for the anatase TiO_2-supported palladium catalyst, but not for the rutile TiO_2-supported catalyst [50]. They found that the Ti^{3+} ions of anatase TiO_2 were generated by the reduction of Ti^{4+} with the dissociatively chemisorbed hydrogen on the Pd diffused into the TiO_2 surface, while rutile TiO_2, which is more structurally stable than anatase TiO_2, could not be reduced at such a low reduction temperature. Previous study presented that the TiO_2 phase of Pd/TiO_2 in SMSI state was reduced to Ti_4O_7 [51], which is also revealed in the Ti 2p spectrum of PCT500.

The Weerachawanasak group stated that the generation of SMSI in Pd/TiO_2 caused electron enrichment of the Pd metal [52]. The deconvolution of the Pd $3d_{5/2}$ XPS spectrum revealed that the

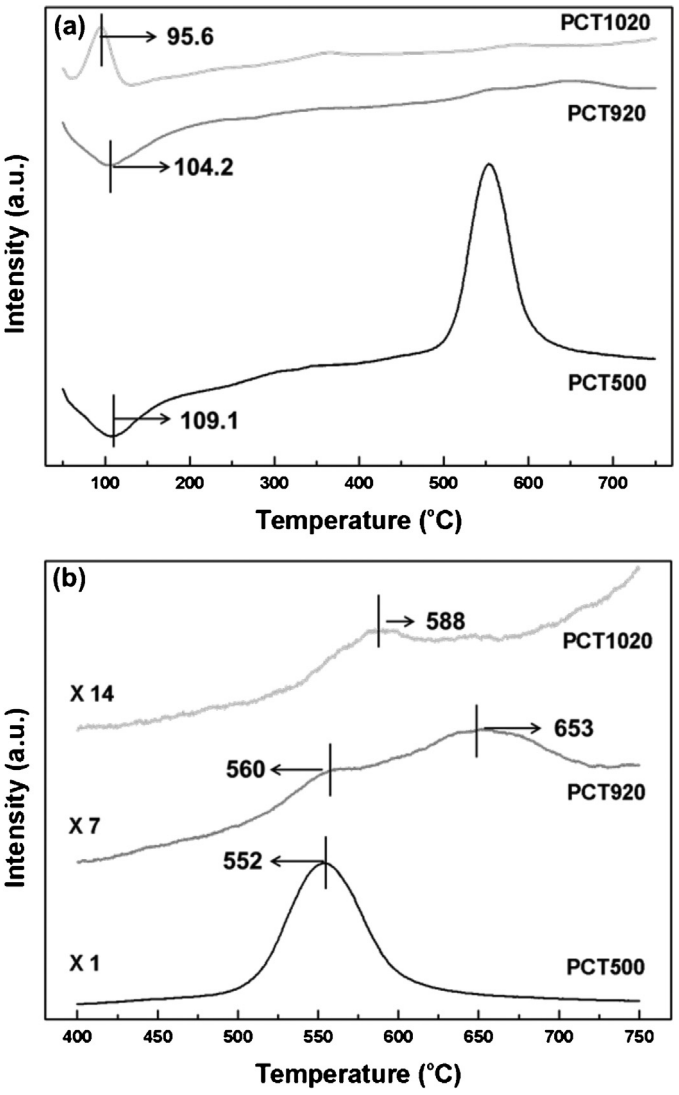

Fig. 3. (a) H_2-TPR profiles of the calcined Pd–Cu/TiO_2 catalysts; (b) magnified H_2-TPR profiles of TiO_2 reduction peak.

lowered binding energy peaks of PCT500 and PCT920 were located at 335.6 and 335.8 eV, respectively (Fig. 4(b)). The values were higher than the binding energy of metallic Pd^0 (335.2 eV), but lower than that of $Pd^{2+}O$. The peak of PCT500 (335.6 eV) was slightly lower-shifted than that of PCT920 (335.8 eV), which indicated that the Pd of PCT500 was more electron rich. For PCT1020, the binding energy of Pd $3d_{5/2}$ was 336.2 eV, which was exactly assigned to $Pd^{2+}O$. This observation might be related to the Ti state in PCT1020 (i.e., Ti^{4+}) because reduction did not occur over rutile TiO_2.

It was similarly observed in the XPS spectra of the Cu species (Fig. 4(c)). Although the multivalent state of Cu complicated the discrimination of distinct Cu species, the deconvoluted peak located at 932.9 eV for PCT500 was close to metallic Cu^0 state (932.8 eV). All or part of the peaks of PCT920 and PCT1020 were attributed to $Cu_2{}^+O$ (932 eV) and $Cu^{2+}O$ (934.1 eV).

The results presented above clearly showed the existence of an SMSI that led to electron transfer from the partially reduced TiO_2 support to the metals. Considering the H_2-TPR patterns and chemical states of the metals and support, SMSI was present in PCT500 and PCT920 and the former was higher than the latter in the degree of interaction. However, an evidence of SMSI was not found for PCT1020.

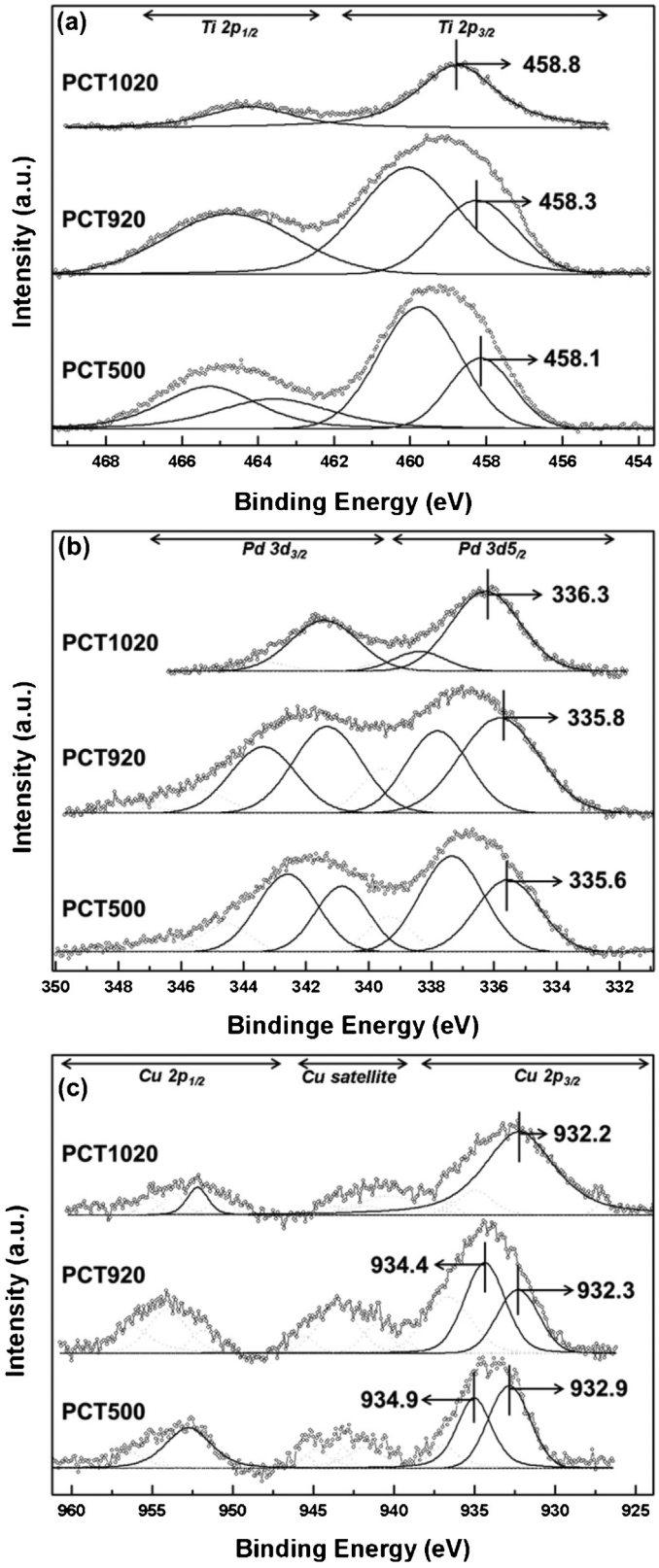

Fig. 4. XPS spectra of Ti 2p (a), Pd 3d (b) and Cu 2p (c) for the reduced Pd–Cu/TiO_2 catalysts.

Table 3
Nitrate conversion and selectivity for nitrite, ammonium and nitrogen in the catalytic nitrate reduction with CO_2 buffer after 100 min of reaction time. Reaction conditions: $C(NO_{3,t=0}^-)$: 2 mM, amount of catalyst: 0.15 g, flow rate of hydrogen: 90 ml/min, flow rate of carbon dioxide: 30 ml/min, T: 25 °C.

Material	$X(NO_3^-)$	$S(NO_2^-)$	$S(NH_4^+)$	$S(N_2)$
PCT500	95	0.3	43.4	56.3
PCT920	27	13.5	45.3	41.2
PCT1020	11	0.4	14.9	84.7

3.4. Reaction tests

To compare the catalytic performance of PCT500, PCT920 and PCT1020, the concentration of nitrate, nitrite and ammonium was estimated under a pure hydrogen flow, which is shown in Fig. 5. Nitrate decreased with reaction time (Fig. 5(a)) and nitrite was formed as the intermediate product (Fig. 5(b)). The ammonium concentration increased as the nitrite was converted. The complete nitrate reduction was achieved in a reaction time of approximately 40 min for PCT500 which was estimated to be 0.5 mmol/min/g_{cat} in the reaction rate. PCT500 was much faster in nitrate reduction rate than Pd–Cu/TiO_2 of other studies (0.05 [30] and 0.36 [31] mmol/min/g_{cat}). On the other hand, the nitrate was slowly diminished over PCT920 than PCT500, and PCT1020 showed the poorest nitrate reduction activity. More ammonium was generated over PCT500 than PCT920 and PCT1020, but the N_2 selectivity of PCT500 and PCT920 was very low (13 and 8%, respectively at 100 min: not shown in the figure). After complete nitrate reduction, the nitrite was slowly consumed (nitrite accumulation), which might be due to the high pH resulting from the production of hydroxide ions in the solution [53]. It is known that high pH negatively influences the N_2 selectivity [54]. Regarding this phenomenon, Yang et al. claimed that the nitrite reduction activity of Pd–Cu/TiO_2 catalysts decreased as pH of reaction medium increased [31]. Furthermore, the formation of ammonium was favored in the high pH environment [55]. Fig. 6 shows the pH values as a function of reaction time over PCT500 and PCT920. It was found that the pH values reached over 12 when the nitrate conversion exceeded approximately 50% (1.0 mM in concentration).

Several researchers have studied the effect of pH on the nitrate reduction activity and concluded that the maximum catalytic performance was achieved at moderate pH values (pH 4–8), depending on the catalysts used [13]. In a related study, bubbling CO_2 into the reaction solution was also evaluated as an efficient method to control pH [56]. Thus, we added CO_2 to the feed gas (H_2) as a pH buffer and observed its influence on the catalytic activity.

The concentration–reaction time profiles for nitrate over PCT500 with CO_2 co-fed into the reaction solution are shown in Fig. 7, which also presents the pH variation during the reaction test. The pH values increased relatively slowly with the reaction time and reached 6, 5.6 and 5.2 at the end of the reaction with flow rate of CO_2 of 10, 30 and 60 ml/min, respectively. Comparison of the nitrate concentration profiles showed that the best result was obtained when CO_2 flow rate was 30 ml/min. Based on this result, we fixed a feed gas composition to H_2:CO_2 = 90:30 ml/min in the following tests.

Table 3 compares the nitrate conversion and the selectivity for nitrite, ammonium and nitrogen of the PCT catalysts obtained after 100 min. A nitrate conversion of 95% was reached over PCT500, while those of PCT920 and PCT1020 were very low (below 30%). The performance was dissimilar to the cases of pure hydrogen condition: Some negative influences of CO_2 feeding were reported on the nitrate reduction activity of Pd catalysts, which were explained to cause from the formation of carbonate or hydrogen carbonate on the support [55,57,58]. However, nitrate was almost completely converted (95%) within the reaction time under CO_2/H_2 condition

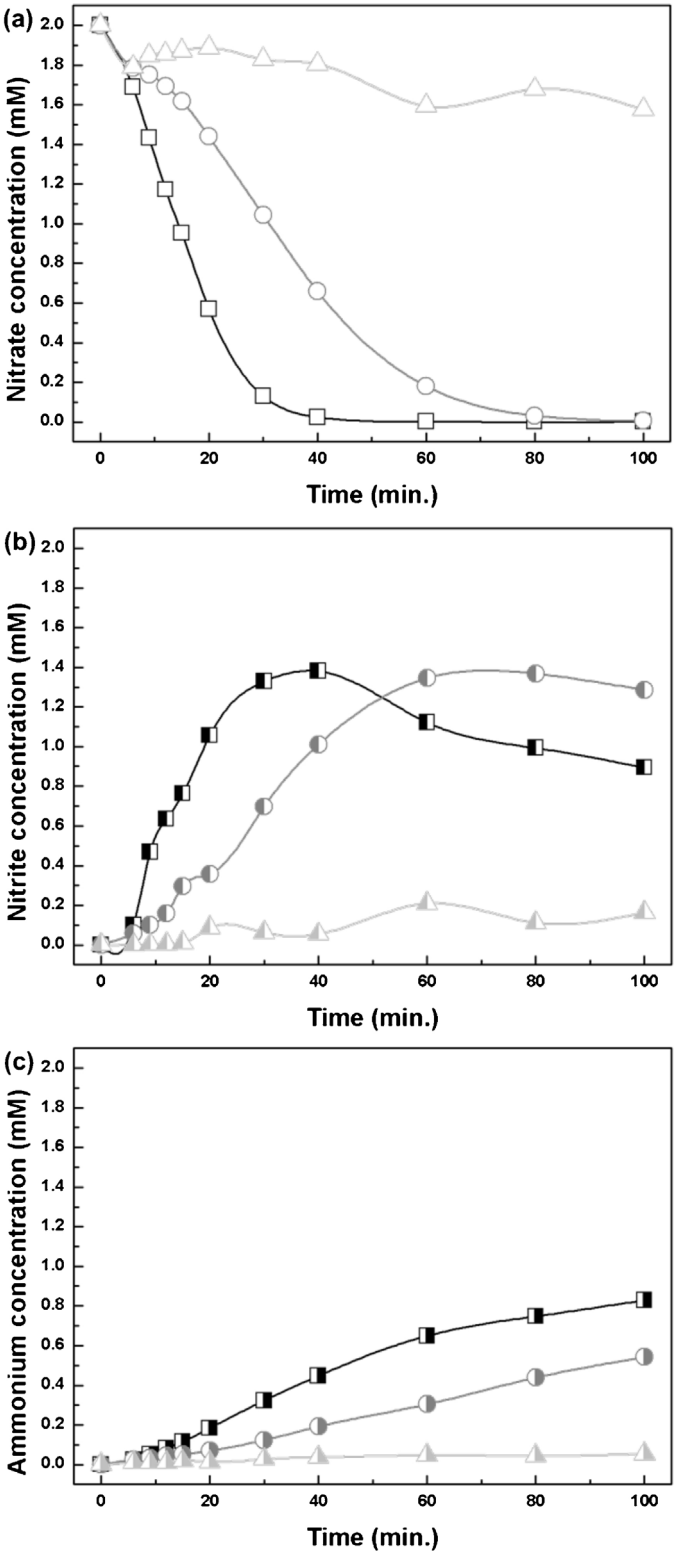

Fig. 5. Nitrate (a), nitrite (b) and ammonium (c) concentrations as a function of reaction time for catalytic nitrate reduction without CO_2 buffer (□: PCT500, ○: PCT920, △:PCT1020). Reaction conditions: $C(NO_{3,t=0}^-)$: 2 mM, amount of catalyst: 0.15 g, flow rate of hydrogen: 90 ml/min, T: 25 °C.

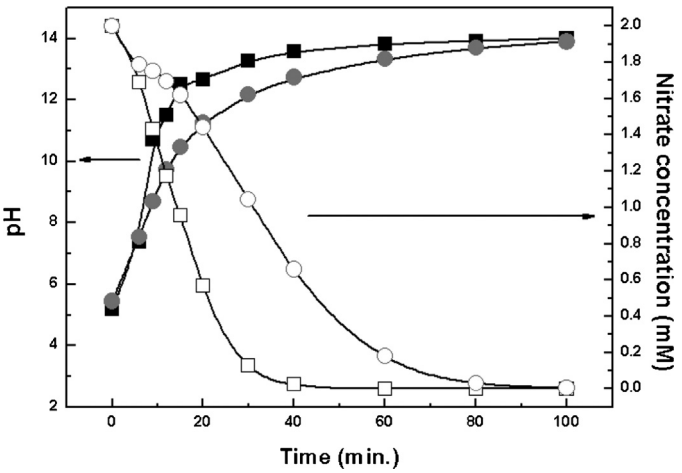

Fig. 6. pH and nitrate concentrations as a function of reaction time over Pd–Cu/TiO_2 catalysts without CO_2 co-feeding (□: PCT500, ○: PCT920).

over PCT500. The remarkable effect of CO_2 bubbling was shown in the nitrite selectivity over PCT500, which drastically diminished nitrite accumulation during the nitrate reduction. As a result, approximately 0.3% of the nitrite selectivity was estimated, which subsequently resulted in increased N_2 selectivity (56%) much higher than that under pure hydrogen conditions. The improvement of N_2 selectivity by CO_2 co-feeding was also observed over the PCT920 and PCT1020, but the selectivities were meaningless because of the low nitrate conversion over both catalysts.

From the results presented above, it was clear that the anatase composition in TiO_2 support significantly influenced the catalytic performance of PCT catalysts in the nitrate reduction. The order of catalytic performance was: PCT500 > PCT920 > PCT1020, which coincided with the trend of the degree in SMSI over the catalysts. SMSI is basically an electronic effect that changed the electronic properties of the metals on the partially reduced TiO_2 supports [44]. With regards to the results of the H_2-TPR and XPS, the Ti species of PCT500, which has the strongest metal-support interaction among the PCT catalysts, revealed the more reduced state (closer to Ti^{3+}), and generates more oxygen vacancy (TiO_{2-x}) on the surface than PCT920 and PCT1020. It was reported that the reactivity of the Ni/TiO_2 catalysts in the hydrogenation of *o*-chloronitrobenzene

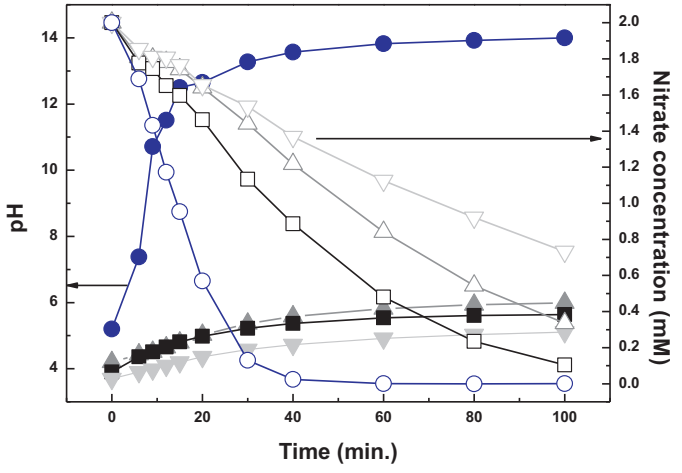

Fig. 7. Effect of CO_2 flow rate on nitrate concentration profiles over PCT500 catalyst (○: 0 ml/min, △: 10 ml/min, □: 30 ml/min, □: 60 ml/min). Reaction conditions: $C(NO_{3,t=0}^{-})$: 2 mM, amount of catalyst: 0.15 g, flow rate of hydrogen: 90 ml/min, *T*: 25 °C.

was affected by the SMSI effect. The explanation for this effect was that the oxygen vacancies of the support could coordinate the oxygen atoms in the N=O group of chloronitrobenzene, and as a result, the polarized N=O band was easily attacked by hydrogen adsorbed on the nickel particles in the vicinity of oxygen vacancies [59]. Similar results were found in the previous studies describing the nitrate hydrogenation activities of Pd-monometallic impregnated on reducible support such as CeO_2 or TiO_2 [57,60]. It was shown that nitrate could be reduced by the interaction of the oxygen atoms of nitrate with the oxygen vacancies (Ce^{3+}, Ti^{3+}) on the reducible support which was formed by H_2 reduction. Guo et al. observed that the TiO_2 doped Pd/SnO_2 catalysts had the increased amount of the oxygen vacancies, which resulted in a superior nitrate reduction activity to the pure Pd/SnO_2 catalysts [61]. These results indicated that the oxygen vacancies on reduced support enhanced the nitrate reduction activity, which was in agreement with the trends observed with the PCT catalysts in this study.

The roles of Cu and Pd in Pd–Cu/TiO_2 catalysts used in nitrate reduction were also considered. Epron et al. reported that the nitrate is reduced into nitrite on the Cu sites with oxidation of metallic Cu to Cu^{2+} which was then reduced back to metallic Cu by hydrogen spilled over from the neighboring Pd [62]. Other studies claimed that Pd was active for converting the nitrite into ammonium ion or nitrogen [63,64]. Through in situ HERFD XAS (High Energy Resolution Fluorescence Detection X-ray Absorption Spectroscopy) study, Sá et al. clearly proved that the metallic Cu was the active site for reducing nitrate into nitrite in Pd–Cu catalysts [65]. In our Cu $2p_{3/2}$ XPS results (Fig. 4(c)), it was found that the Cu species in PCT500 was very close to metallic Cu, while those of other catalysts (PCT920 and PCT1020) proved to be Cu oxides. It is expected that the metallic Cu is crucial for the nitrate reduction activity of PCT500.

Based on the discussions so far, we expected that the nitrate reduction over PCT500 progressed as follows: Nitrate was first adsorbed on the oxygen vacancies of TiO_{2-x} in the vicinity of Pd and Cu. Then, the weakly bound nitrate was converted into nitrite on the metallic Cu which is oxidized to Cu^{2+} through the conversion. The converted nitrite was migrated to Pd on which the nitrite was reduced to ammonium or nitrogen. The oxidized Cu was reduced back to metallic Cu by hydrogen spilled over from Pd, which completed a redox cycle.

4. Conclusions

The composition of the crystalline anatase phase of the TiO_2 supports has a great influence on the catalytic performance. As revealed by H_2-TPR and XPS analysis, Pd–Cu/TiO_2 catalysts containing more anatase fractions produced stronger metal-support interactions through treatment by H_2 reduction. Based on the SMSI effect, the partially reduced TiO_2 support enriched the electrons of Pd and Cu, which was beneficial to the nitrate reduction activity. As a result, nitrate rapidly converted into nitrite over PCT500 under pure hydrogen flow, whereas PCT920 and PCT1020 displayed little or no metal-support interaction and presented lower activity. However, it was necessary to use a pH buffer to promote the activity, because the nitrite accumulation led to poor N_2 selectivity under pure hydrogen flow. Using CO_2 as the pH buffer, we obtained an improved N_2 selectivity. Although nitrate reduction occurred rather slowly, PCT500 still exhibited the best catalytic performance. After 100 min of reaction time, the catalyst achieved 95% nitrite conversion and 56% N_2 selectivity under H_2/CO_2 flow. Based on the results presented above, we could conclude that SMSI induced from anatase-dominant TiO_2 support was crucial in promoting the activity of Pd–Cu/TiO_2 catalysts for nitrate reduction.

Acknowledgment

This work is supported by Korea Ministry of Environment as "Global Top Project" (Project No.: GT-11-B-01-007-0).

References

[1] A. Garron, K. Lázár, F. Epron, Applied Catalysis B 59 (2005) 57–69.
[2] M. Cho, S. Ahn, Korean Journal of Chemical Engineering 29 (8) (2012) 1057–1062.
[3] C.-P. Huang, H.-W. Wang, P.-C. Chiu, Water Research 32 (8) (1998) 2257–2264.
[4] R. Gavagnin, L. Biasetto, F. Pinna, G. Strukul, Applied Catalysis B 38 (2002) 91–99.
[5] Z. Xu, L. Chen, Y. Shao, D. Yin, S. Zheng, Industrial and Engineering Chemistry Research 48 (2009) 8356–8363.
[6] A. Kapoor, T. Viraraghavan, Journal of Environment Engineering 123 (1997) 371–380.
[7] ARCHNA, S.K. Sharma, R.C. Sobti, European Journal of Chemistry 9 (4) (2012) 1667–1675.
[8] S. Hörold, K.-D. Vorlop, T. Tacke, M. Sell, Catalysis Today 17 (1993) 21–30.
[9] N. Barrabés, J. Just, A. Dafinov, F. Medina, J.L.G. Fierro, J.E. Sueiras, P. Salagre, Y. Cesteros, Applied Catalysis B 62 (2006) 77–85.
[10] H. Liu, C. Yoo, Korean Journal of Chemical Engineering 28 (3) (2011) 667–673.
[11] A. Pintar, J. Batista, Catalysis Today 53 (1999) 35–50.
[12] K.-D. Vorlop, T. Tacke, Chemie Ingenieur Technik 61 (10) (1989) 836–837.
[13] Y.-X. Chen, Y. Zhang, G.-H. Chen, Water Research 37 (2003) 2489–2495.
[14] Y.I. Matatov-Meytal, M. Sheintuch, Industrial and Engineering Chemistry Research 37 (1998) 309–326.
[15] N. Barrabés, J. Sá, Applied Catalysis B 104 (2011) 1–5.
[16] U. Prüsse, K.-D. Vorlop, Journal of Molecular Catalysis A: Chemical 173 (2001) 313–328.
[17] I. Mikami, Y. Sakamoto, Y. Yoshinaga, T. Okuhara, Applied Catalysis B 44 (2003) 79–86.
[18] Y. Yoshinagana, T. Akita, I. Mikami, T. Okuhara, Journal of Catalysis 207 (2002) 37–45.
[19] O.S.G.P. Soares, J.J.M. Órfão, M.F.R. Pereira, Applied Catalysis B 91 (2009) 441–448.
[20] B.P. Chaplin, E. Roundy, K.A. Guy, J.R. Shapley, C.J. Werth, Environmental Science and Technology 40 (2006) 3075–3081.
[21] D. Gašparovičová, M. Králik, M. Hronec, A. Biffis, M. Zecca, B. Corain, Journal of Molecular Catalysis A: Chemical 244 (2006) 258–266.
[22] D. Gašparovičová, M. Králik, M. Hronec, Z. Vallušová, H. Vinek, B. Corain, Journal of Molecular Catalysis A: Chemical 264 (2007) 93–102.
[23] A. Aristizábal, S. Contreras, N. Barrabés, J. Llorca, D. Tichit, F. Medina, Applied Catalysis B 110 (2011) 58–70.
[24] M. Al Bahri, L. Calvo, M.A. Gilarranz, J.J. Rodriguez, F. Epron, Applied Catalysis B 139 (2013) 141–148.
[25] L. Lemaignen, C. Tong, V. Begon, R. Burch, D. Chadwik, Catalysis Today 75 (2002) 43–48.
[26] T. Yuranova, C. Franch, A.E. Palomares, E. Garcia-Bordejé, L. Kiwi-Minsker, Applied Catalysis B 123–124 (2012) 221–228.
[27] C. Neyertz, F.A. Marchesini, A. Boix, E. Miró, C.A. Querini, Applied Catalysis A 372 (2010) 40–47.
[28] M.P. Maia, M.A. Rodrigues, F.B. Passos, Catalysis Today 123 (2007) 171–176.
[29] C.P. Theologides, P.G. Savva, C.N. Costa, Applied Catalysis B 102 (2011) 54–61.
[30] W. Gao, N. Guan, J. Chen, X. Guan, R. Jin, H. Zeng, Z. Liu, F. Zhang, Applied Catalysis B 46 (2003) 341–351.
[31] D. Yang, W. Feng, G. Wu, L. Li, N. Guan, Catalysis Today 175 (2011) 356–361.
[32] F. Zhang, S. Miao, Y. Yang, X. Zhang, J. Chen, N. Guan, Journal of Physical Chemistry C 112 (2008) 7665–7671.
[33] S.C. Fung, Journal of Catalysis 76 (1982) 225–230.
[34] S.J. Tauster, S.C. Fung, R.L. Garten, Journal of the American Chemical Society 100 (1978) 170–175.
[35] D.C. Grenoble, Journal of Catalysis 56 (1979) 32–39.
[36] U.K. Singh, M.A. Vannice, Journal of Molecular Catalysis A: Chemical 163 (2000) 233–250.
[37] J. Santos, J. Phillips, J.A. Dumesic, Journal of Catalysis 81 (1983) 147–167.
[38] G.B. Raupp, J.A. Dumesic, Journal of Catalysis 95 (1985) 587–601.
[39] J.M. Herrmann, M.G.-R. Maillot, P.C. Gravelle, Journal of Catalysis 104 (1987) 136–146.
[40] P. Chou, M.A. Vannice, Journal of Catalysis 104 (1987) 1–16.
[41] P. Reyes, H. Rojas, G. Pecchi, J.L.G. Fierro, Journal of Molecular Catalysis A: Chemical 179 (2002) 293–299.
[42] Y. Li, B. xu, Y. Fan, N. Feng, A. Qiu, J.M.J. He, H. Yang, Y. Chen, Journal of Molecular Catalysis A: Chemical 216 (2004) 107–114.
[43] K.J.A. Raj, M.G. Prakash, R. Mahalakshmy, T. Elangovan, B. Viswanathan, Catalysis Science and Technology 2 (2012) 1429–1436.
[44] J. Panpranot, K. Kontapakdee, P. Praserthdam, Journal of Physical Chemistry B 110 (2006) 8019–8024.
[45] W.-J. Shen, M. Okumura, Y. Matsumura, M. Haruta, Applied Catalysis A 213 (2001) 225–232.
[46] M.P. Kapoor, Y. Ichihashi, K. Kuraoka, Y. Matsumura, Journal of Molecular Catalysis A: Chemical 198 (2003) 303–308.
[47] I. Witońska, S. Karski, J. Rogowski, N. Krawczyk, Journal of Molecular Catalysis A: Chemical 287 (2008) 87–94.
[48] J. Sá, G.D. Arteaga, R.A. Daley, J. Bernardi, J.A. Anderson, Journal of Physical Chemistry B 110 (2006) 17090–17095.
[49] J. Xu, K. Sun, L. Zhang, Y. Ren, X. Xu, Catalysis Communications 6 (2005) 462–465.
[50] Y. Li, Y. Fan, H. Yang, B. Xu, L. Feng, M. Yang, Y. Chen, Chemical Physics Letters 372 (2003) 160–165.
[51] J. Sá, J. Bernardi, J.A. Anderson, Catalysis Letters 114 (1-2) (2007) 91–95.
[52] P. Weerachawanasak, O. Mekasuwandumrong, M. Arai, S.-I. Fujita, P. Praserthdam, J. Panpranot, Journal of Catalysis 262 (2009) 199–205.
[53] I. Dodouche, D.P. Barbosa, M.D.C. Rangel, F. Epron, Applied Catalysis B 93 (2009) 50–55.
[54] G. Strukul, R. Gavagnin, F. Pinna, E. Modaferri, S. Perathoner, G. Centi, M. Marella, M. Tomaselli, Catalysis Today 55 (2000) 139–149.
[55] A. Devadas, S. Vasudevan, F. Epron, Journal of Hazardous Materials 185 (1) (2011) 1412–1417.
[56] M. D'Arino, F. Pinna, G. Strukul, Applied Catalysis B 53 (2004) 161–168.
[57] F. Epron, F. Gauthard, J. Barbier, Journal of Catalysis 206 (2002) 363–367.
[58] C. Binet, M. Daturi, J.-C. Lavalley, Catalysis Today 50 (1999) 207–225.
[59] J. Xiong, J. Chen, J. Zhang, Catalysis Communications 8 (2007) 345–350.
[60] J. Sá, T. Berger, K. Föttinger, A. Riss, J.A. Anderson, H. Vinek, Journal of Catalysis 234 (2005) 282–291.
[61] Y.-n. Guo, J.-h. Cheng, Y.-y. Hu, D.-h. Li, Applied Catalysis B 125 (2012) 21–27.
[62] F. Epron, F. Gauthard, C. Pinéda, J. Barbier, Journal of Catalysis 198 (2001) 309–318.
[63] O.S.G.P. Soares, J.J.M. Órfão, M.F.R. Pereira, Applied Catalysis B 102 (2011) 424–432.
[64] J. Jung, S. Bae, W. Lee, Applied Catalysis B 127 (2012) 148–158.
[65] J. Sá, N. Barrabés, E. Kleymenov, C. Lin, K. Föttinger, O.V. Safonova, J. Szlachetko, J.A.v. Bokhoven, M. Nachtegaal, A. Urakawa, G.A. Crespo, G. Rupprechter, Catalysis Science and Technology 2 (2012) 794–799.